J|A|C|S
ARTICLES
Published on Web 02/25/2004

# Electronic Structure of Tubular Aromatic Molecules Derived from the Metallic (5,5) Armchair Single Wall Carbon Nanotube

Zhiyong Zhou,[†] Michael Steigerwald,[‡] Mark Hybertsen,[§] Louis Brus,*[,†] and Richard A. Friesner[†]

*Contribution from the Department of Chemistry, Materials Research Science and Engineering Center, and Department of Applied Physics and Applied Mathematics and Columbia Center for Electron Transport in Molecular Nanostructures, Columbia University, New York, New York 10027*

Received October 28, 2003; E-mail: brus@chem.columbia.edu

***Abstract:*** All-electron static and time-dependent DFT electronic calculations, with complete geometrical optimization, are performed on tubular molecules up to $C_{210}H_{20}$ that are finite sections of the (5,5) metallic single wall carbon nanotube with hydrogen termination at the open ends. We find pronounced C−C bond reconstruction at the tube ends; this initiates bond alternation that propagates into the tube centers. For the especially low band gap molecules $C_{120}H_{20}$, $C_{150}H_{20}$, and $C_{180}H_{20}$, alternation increases, and a second nearly isoenergic structural isomer of different alternation is found. A small residual C−C bond alternation and band gap may be present in the infinite tube. The van Hove band gap forms quickly with length, while the metallic Fermi point (at the crossing of linear bands) forms very slowly with length. There are no end-localized states at energies near the Fermi energy. The HOMO−LUMO gap and the lowest singlet excited state, whose energies show a periodicity with length as previously calculated, are optically forbidden. However, each molecule shows an intense visible "charge transfer" transition, not present in the infinite tube, whose energy varies smoothly with length; this transition should be an identifying signature for these molecules. The static axial polarizability per unit length increases rapidly with $N$ as the "charge transfer" transition moves into the infrared; this indicates increasing metallic character. However, the ionization potential, electron affinity, chemical hardness, and relative energetic stability all show the length periodicity seen in the HOMO−LUMO gap, in contrast to the optical "charge transfer" transition and the static axial polarizability. These periodicities, due to a one-dimensional quantum size effect as originally modeled by Coulson in 1938, nevertheless cancel in the calculated Fermi energy, which varies smoothly toward a predicted bulk work function near 3.9 eV. A detailed study of $C_{190}H_{20}$ with up to eight extra electrons or holes shows the total energy is closely fit by a simple classical charging model, as is commonly applied to metallic clusters.

## Introduction and Methods

Single wall carbon nanotubes (SWNTs) are among the most interesting new materials discovered in many years. Grown catalytically at high temperature in the gas phase, they can be almost structurally perfect and show ballistic electron motion at 23 °C over lengths of several micrometers. This near structural perfection, coupled with physical rigidity and weak vibronic coupling as compared to other conjugated aromatic polymers, makes them ideal for fundamental studies of electrons in one dimension.

Infinite length SWNTs are $\pi$-bonded aromatic molecules that can be either semiconducting or metallic, depending upon the diameter and helical angle. In a pioneering 1992 DFT calculation, Mintmire, Dunlap, and White[1] predicted the infinite length (5,5) armchair SWNT (0.67 nm diameter) would be metallic with a very low transition temperature separating the uniform (high temperature) structure from the Peierls bond alternating (low temperature) structure. This specific SWNT is the elongated tube of the $C_{60}$, $C_{70}$, etc., molecular family. SWNT electronic structure can also be simply understood using the most elementary topological Hückel (tight binding) molecular orbital (MO) analysis.[2] In Figure 1, two locally linear bands cross at an electron Fermi momentum $k_F$ (along the axis) of about two-thirds of the zone boundary; the Fermi energy occurs at this point in the neutral infinite metallic tube.[3] The $\mu$ band labels shown correspond to different quantized values of electron momentum around the circumference. While the linear crossing bands dominate electron transport, the optical properties are dominated by a strong peak (van Hove transition) at the absorption threshold between the $\mu = 4$ and $\mu = 6$ bands at 3.1 eV in this figure. The infinite (5,5) SWNT is an unusual type

[†] Department of Chemistry.
[‡] Materials Research Science and Engineering Center.
[§] Department of Applied Physics and Applied Mathematics and Columbia Center for Electron Transport in Molecular Nanostructures.

(1) Mintmire, J. W.; Dunlap, B. I.; White, C. T. *Phys. Rev. Lett.* **1992**, *68*, 631.
(2) Saito, R.; Fujita, M.; Dresselhaus, G.; Dresselhaus, M. S. *Phys. Rev. B* **1992**, *46*, 1804.
(3) Ding, J. W.; Yan, X. H.; Cao, J. X. *Phys. Rev. B* **2002**, *66*, 073401.

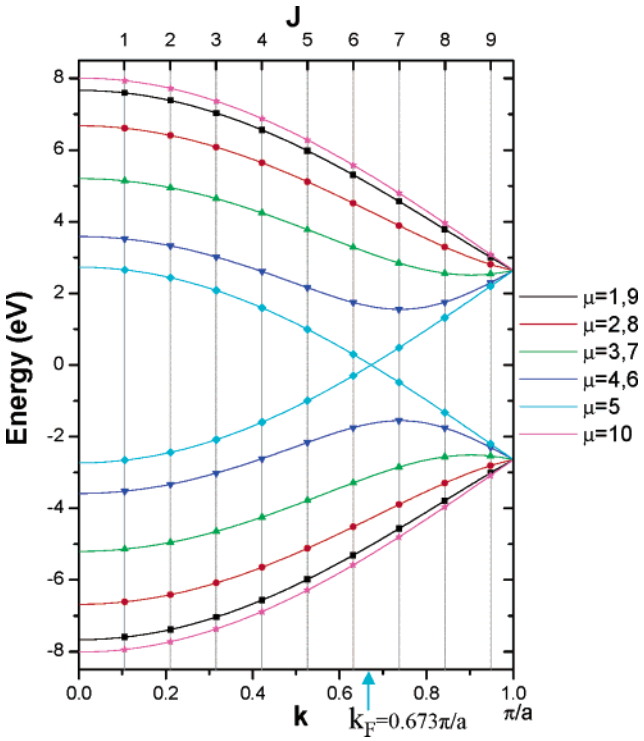


***Figure 1.*** Continuous bands for (5,5) SWNT calculated using a curvature-modified tight binding model (ref 3). The Hückel resonance integral 2.7 eV is used to plot this figure. Points give quantized energy levels for $C_{180}H_{20}$ in the Coulson model.

of metal, in that the optical spectrum is molecule-like with a transparent region below a strong apparently discrete transition. This strong optical transition is experimentally used for structural identification, in direct optical absorption, and in resonance Raman scattering.[4]

In this paper, we consider how the electronic structures of short molecular sections of the (5,5) tube relate to, differ from, and asymptotically approach the infinite metallic tube. Such cylindrical aromatic molecules have not yet been made with the exception of a derivative of $C_{40}H_{20}$.[5] We predict structural, optical, and charge storage properties for this family of molecules. In the (5,5) tube, the structure can be built up by successively adjoining sections of 10 C atoms. In the infinite tube, the periodic unit cell is two such sections consisting of 20 C atoms.[6] Consider the $C_{180}H_{20}$ molecule made from 18 sections or 9 unit cells with the ends capped with H atoms. This species will have discrete MO levels resulting from quantum confinement along the length $L$. In 1938, C. A. Coulson analytically solved the Hückel problem in one dimension, showing how discrete MOs evolve into continuous bands as the length of a conjugated polyolefin chain increases.[7] For such a linear molecule with $N$ states, the $N$ MO energies lie on the continuous bands at discrete momentum ratios $J/(N+1)$ to the zone boundary, where $J$ is a longitudinal quantum number in the range 1,2,...$N$. The crossing bands near the Fermi level in Figure 1 ($\mu = 5$ and $\mu = 10$ bands) can be exactly mapped onto the Coulson model where each of the $N$ states is extended around the circumference of one section. However, the zone boundary in the Coulson model references the section spacing ($a/2$), while the band structure for the (5,5) tube conventionally is plotted in the Brillouin zone for the unit cell spacing ($a$). This leads to a folding of these bands in Figure 1 (the $\mu = 5$ bands continue as the $\mu = 10$ bands), and the Coulson model predicts the allowed states at $2J\pi/(N+1)a$ for $J = 1,2,...,N/2$,[8] where $N$ is the number of 10 C atom sections. Figure 1 shows these predicted energies for $N = 18$; the $J = 6$ and 7 momenta fall on either side of the Fermi momentum $k_F = 0.673\pi/a$.[9] In the absence of an accidental coincidence with $k_F$, a finite length (5,5) tube has a band gap. As seen from analysis of the Coulson momentum factor, there is a near coincidence with $k_F$ every third value of $N$ as $N$ increases. As $L$ increases, the band gap tends to zero, with a superimposed oscillation of $\Delta N = 3$. This oscillation is in fact seen in earlier calculations on finite (5,5) tubes.[10−13] The oscillatory aspect of the quantum size effect is absent in materials that have a Fermi energy or band gap at the zone extrema, such as the (9,0) metallic SWNT or typical 3D semiconductor nanocrystals.

How valid is this picture in actual (5,5) fragments? We attempt to address this using the substantial advances in electronic structure methods based on density functional theory (DFT) that have occurred in the past decade. We use static and time-dependent DFT (TD-DFT) and independently optimize structure for neutrals, cations, and anions. We employ the hybrid nonlocal B3LYP functional. In comparison with LDA and pure GGA functionals, this class of functional has significantly improved calculation of both quantitative energetics in small molecules[14,15] and quantitative optical properties of simple and complex (multielement oxide) crystals.[16−18] Large-scale numerical calculations are now feasible due to a major increase in coding efficiency, and to the remarkable increase of power in low cost PCs.

**Calibration of Methods and $C_{60}$ Electronic Structure.** Static DFT calculations were done using Jaguar 5.0;[19] TD-DFT calculations were done using Q-Chem 2.0 in the Tamm−Dancoff approximation.[20] To calibrate electronic energies, we first compare calculated ionization properties of $C_{60}$ to experimental values. With complete geometrical optimization of radical cation, radical anion, and neutral, we calculate an

(4) Yu, Z. H.; Brus, L. E. *J. Phys. Chem. B* **2001**, *105*, 6831.
(5) Nakamura, E.; Tahara, K.; Matsuo, Y.; Sawamura, M. *J. Am. Chem. Soc.* **2003**, *125*, 2834.
(6) Even values of $N$ correspond to discrete numbers of bulk unit cells and show $D_{5d}$ symmetry. Species such as $C_{50}H_{20}$ correspond to odd values of $N$; they show $D_{5h}$ symmetry.
(7) Coulson, C. A. *Proc. R. Soc. London, Ser. A* **1938**, *164*, 383.
(8) The Coulson model is equivalent to assuming that the wave functions have nodes on the missing sections beyond the tube ends. In applying the Coulson model to all of the states in Figure 1, we are generalizing to the usual envelope function model and applying this nodal condition. For odd $N$, $J$ values up to $(N+1)/2$ are included. We also neglect mixing between states of the same symmetry coming from different bands.
(9) When curvature is not considered, the Fermi momentum is exactly $^2/_3$ of the zone boundary.
(10) Rochefort, A.; Salahub, D. R.; Avouris, P. *J. Phys. Chem. B* **1999**, *103*, 641.
(11) Yamabe, T.; Imade, M.; Tanaka, M.; Sato, T. *Synth. Met.* **2001**, *117*, 61.
(12) Cioslowski, J.; Rao, N.; Moncrieff, D. *J. Am. Chem. Soc.* **2002**, *124*, 8485.
(13) Li, J. Q.; Zhang, Y. F.; Zhang, M. X. *Chem. Phys. Lett.* **2002**, *364*, 338.
(14) Becke, A. D. *J. Chem. Phys.* **1993**, *98*, 5648.
(15) Raghavachari, K. *Theor. Chem. Acc.* **2000**, *103*, 361.
(16) Muscat, J.; Wander, A.; Harrison, N. M. *Chem. Phys. Lett.* **2001**, *342*, 397.
(17) Perry, J. K.; Tahir-Kheli, J.; Goddard, W. A. *Phys. Rev. B* **2002**, *65*, 144501.
(18) Kudin, K. N.; Scuseria, G. E.; Martin, R. L. *Phys. Rev. Lett.* **2002**, *89*, 266402.
(19) Jaguar 5.0, Schrodinger, L.L.C., Portland, OR, 1991−2003.
(20) Q-Chem 2.0: A high-performance ab initio electronic structure program: Kong, J.; White, C. A.; Krylov, A. I.; Sherrill, D.; Adamson, R. D.; Furlani, T. R.; Lee, M. S.; Lee, A. M.; Gwaltney, S. R.; Adams, T. R.; Ochsenfeld, C.; Gilbert, A. T. B.; Kedziora, G. S.; Rassolov, V. A.; Maurice, D. R.; Nair, N.; Shao, Y.; Besley, N. A.; Maslen, P. E.; Dombroski, J. P.; Daschel, H.; Zhang, W.; Korambath, P. P.; Baker, J.; Byrd, E. F. C.; Van Voorhis, T.; Oumi, M.; Hirata, S.; Hsu, C.-P.; Ishikawa, N.; Florian, J.; Warshel, A.; Johnson, B. G.; Gill, P. M. W.; Head-Gordon, M.; Pople, J. A. *J. Comput. Chem.* **2000**, *21*, 1532−1548.

***Table 1.*** Properties of Structurally Optimized (5,5) CNT Fragments As Described in the Text[a]

| | $C_{20}H_{20}$ | $C_{30}H_{20}$ | $C_{40}H_{20}$ | $C_{50}H_{20}$ | $C_{60}H_{20}$ | $C_{70}H_{20}$ | $C_{80}H_{20}$ | $C_{90}H_{20}$ | $C_{100}H_{20}$ | $C_{110}H_{20}$ |
|---|---|---|---|---|---|---|---|---|---|---|
| symmetry of fragment | $D_{5d}$ | $D_{5h}$ | $D_{5d}$ | $D_{5h}$ | $D_{5d}$ | $D_{5h}$ | $D_{5d}$ | $D_{5h}$ | $D_{5d}$ | $D_{5h}$ |
| length of fragment (Å) | 1.23 | 2.46 | 3.69 | 4.92 | 6.15 | 7.38 | 8.61 | 9.84 | 11.07 | 12.30 |
| HOMO | −5.02 | −4.56 | −4.83 | −4.39 | −4.17 | −4.50 | −4.28 | −4.02 | −4.32 | −4.24 |
| symmetry of HOMO | a2u | a2′ | a1u | a2″ | a2g | a1″ | a2u | a2′ | a1u | a2″ |
| LUMO | −1.44 | −2.08 | −1.79 | −2.18 | −2.61 | −2.30 | −2.55 | −2.91 | −2.63 | −2.74 |
| symmetry of LUMO | a1u | a1′ | a2u | a1″ | a1g | a2″ | a1u | a1′ | a2u | a1″ |
| LUMO−HOMO gap Δ | 3.58 | 2.48 | 3.04 | 2.21 | 1.56 | 2.20 | 1.73 | 1.11 | 1.70 | 1.51 |
| adiabatic ionization potential $I_{pa}$ | 6.27 | 5.73 | 5.96 | 5.47 | 5.17 | 5.48 | 5.24 | 4.94 | 5.23 | 5.09 |
| vertical ionization potential $I_{pv}$ | 6.39 | 5.87 | 6.07 | 5.54 | 5.27 | 5.56 | 5.28 | 4.98 | 5.25 | 5.14 |
| hole reorganization energy $\lambda_h$ | 0.12 | 0.14 | 0.11 | 0.07 | 0.09 | 0.08 | 0.04 | 0.04 | 0.03 | 0.05 |
| adiabatic electron affinity $E_{aa}$ | 0.34 | 0.89 | 0.67 | 1.14 | 1.56 | 1.34 | 1.61 | 1.98 | 1.71 | 1.91 |
| vertical electron affinity $E_{av}$ | 0.08 | 0.78 | 0.57 | 1.03 | 1.51 | 1.25 | 1.55 | 1.94 | 1.69 | 1.84 |
| electron reorganization energy $\lambda_e$ | 0.26 | 0.11 | 0.10 | 0.11 | 0.05 | 0.08 | 0.06 | 0.04 | 0.02 | 0.07 |
| Fermi energy $E_f$ | −3.23 | −3.33 | −3.32 | −3.29 | −3.39 | −3.41 | −3.42 | −3.46 | −3.47 | −3.49 |
| absolute hardness $\eta$ | 6.31 | 5.08 | 5.50 | 4.51 | 3.75 | 4.31 | 3.73 | 3.04 | 3.56 | 3.30 |
| polarizability $\alpha_{zz}$ ($10^{-39}$ C V$^{-1}$ m$^2$) | 0.11 | 0.44 | 1.00 | 1.56 | 1.80 | 3.48 | 5.21 | 5.94 | 7.85 | 10.24 |
| | $C_{120}H_{20}$ | $C_{130}H_{20}$ | $C_{140}H_{20}$ | $C_{150}H_{20}$ | $C_{160}H_{20}$ | $C_{170}H_{20}$ | $C_{180}H_{20}$ | $C_{190}H_{20}$ | $C_{200}H_{20}$ | $C_{210}H_{20}$ |
| symmetry of fragment | $D_{5d}$ | $D_{5h}$ | $D_{5d}$ | $D_{5h}$ | $D_{5d}$ | $D_{5h}$ | $D_{5d}$ | $D_{5h}$ | $D_{5d}$ | $D_{5h}$ |
| length of fragment (Å) | 13.53 | 14.76 | 15.99 | 17.22 | 18.45 | 19.68 | 20.91 | 22.14 | 23.37 | 24.60 |
| HOMO | −3.96 | −4.18 | −4.21 | −3.93 | −4.14 | −4.19 | −3.94 | −4.07 | −4.20 | −3.97 |
| symmetry of HOMO | a2g | a1″ | a2u | a2′ | a1u | a2″ | a1g | a1″ | a2u | a1′ |
| LUMO | −3.08 | −2.87 | −2.88 | −3.20 | −3.00 | −2.98 | −3.24 | −3.13 | −3.02 | −3.27 |
| symmetry of LUMO | a1g | a2″ | a1u | a1′ | a2u | a1″ | a2g | a2″ | a1u | a2′ |
| LUMO−HOMO gap Δ | 0.88 | 1.30 | 1.33 | 0.73 | 1.14 | 1.21 | 0.70 | 0.93 | 1.17 | 0.70 |
| adiabatic ionization potential $I_{pa}$ | 4.81 | 4.98 | 4.99 | 4.69 | 4.82 | 4.92 | 4.65 | 4.72 | | |
| vertical ionization potential $I_{pv}$ | 4.83 | 5.02 | 5.00 | 4.74 | 4.90 | 4.95 | 4.68 | 4.79 | 4.91 | 4.63 |
| hole reorganization energy $\lambda_h$ | 0.01 | 0.04 | 0.01 | 0.05 | 0.08 | 0.02 | 0.03 | 0.07 | | |
| adiabatic electron affinity $E_{aa}$ | 2.24 | 2.06 | 2.13 | 2.43 | 2.35 | 2.23 | 2.53 | 2.45 | | |
| vertical electron affinity $E_{av}$ | 2.21 | 2.02 | 2.07 | 2.40 | 2.25 | 2.23 | 2.49 | 2.42 | 2.32 | 2.60 |
| electron reorganization energy $\lambda_e$ | 0.03 | 0.04 | 0.06 | 0.03 | 0.10 | 0.01 | 0.03 | 0.04 | | |
| Fermi energy $E_f$ | −3.52 | −3.52 | −3.54 | −3.57 | −3.57 | −3.59 | −3.59 | −3.60 | −3.62 | −3.61 |
| absolute hardness $\eta$ | 2.62 | 2.99 | 2.93 | 2.34 | 2.65 | 2.72 | 2.19 | 2.37 | 2.59 | 2.03 |
| polarizability $\alpha_{zz}$ ($10^{-39}$ C V$^{-1}$ m$^2$) | 11.15 | 15.38 | 17.56 | 18.91 | 25.99 | 27.93 | 33.43 | 38.09 | 43.58 | 45.14 |

[a] All energies are in eV. All species were calculated at the 6-31g* level.

adiabatic electron affinity of 2.05 eV (2.50 eV) with 6-31g* (cc-pvtz(-f)) basis sets. Similarly, the adiabatic ionization potential is 7.16 eV (7.44 eV). The larger basis numbers compare well to both the experimental electron affinity of 2.689 eV[21] and the experimental ionization potential which has been placed near 7.54 eV.[22]

The nanotube optical transitions should be pure valence $\pi-\pi^*$. In general, TD-DFT has accurately reproduced low-lying $\pi-\pi^*$ optical spectra in $C_{60}$,[23] oligothiophenes,[24,25] ladder-type oligomers,[26] polycyclic aromatics,[27] and planar heteroaromatic molecules,[28−30] often to within 0.2 eV. In a recent study of the large planar aromatics $C_{20}H_{12}$, $C_{30}H_{16}$, and $C_{40}H_{20}$, the 6-31g* basis which we use for SWNTs below gave accurate TD-DFT comparisons to the measured optical spectra.[31]

An important question is the accurate prediction of vibronic (Peierls) bond alternation in extended $\pi$ systems. In a detailed DFT study of this question, the admixture of exact exchange in B3LYP increased predicted bond alternation and improved agreement with experiment in oligoenes and polyacetylene, as compared to the BLYP and especially LDA.[32] The B3LYP DFT result agrees well with MP2; the predicted bond alternation is at the low end of the reported experimental values.[33]

## Results

**Bond Alternation, Band Gap, and Stability.** With the 6-31g* basis in Jaguar 5.0, we have been able to converge all-electron DFT structures up to $C_{210}H_{20}$, with optimization of all structural degrees of freedom. We do not assume any symmetry. Calculated properties appear in Table 1. The calculation for $C_{210}H_{20}$ takes 120 h on a 1.4 GHz Pentium III single processor with 1 GB memory, when starting from the rolled-up graphite geometry. The optimized structures show a large bond alternation whose magnitude varies along the length. For all lengths, the bond alternation patterns are symmetric with respect to the tube center, and the optimized structures are $D_{5d}$ or $D_{5h}$ for $N$ even and odd, respectively, just as would be the case if there were no bond alternation. In infinite armchair tubes, there are two types of bonds: perpendicular to the tube axis (labeled b1) and partially along the axis (b2) as shown in Figure 2. Many previous calculations have only considered a rolled-up graphite structure without structural optimization. A semiempirical

(21) Wang, X. B.; Ding, C. F.; Wang, L. S. *J. Chem. Phys.* **1999**, *110*, 8217.
(22) Rudolf', P.; Golden, M. S.; Bruhwiler, P. A. *J. Electron Spectrosc. Relat. Phenom.* **1999**, *100*, 409.
(23) Bauernschmitt, R.; Ahlrichs, R.; Hennrich, F. H.; Kappes, M. M. *J. Am. Chem. Soc.* **1998**, *120*, 5052.
(24) Gao, Y.; Liu, C. G.; Jiang, Y. S. *J. Phys. Chem. A* **2002**, *106*, 5380.
(25) Telesca, R.; Bolink, H.; Yunoki, S.; Hadziioannou, G.; Van Duijnen, P. T.; Snijders, J. G.; Jonkman, H. T.; Sawatzky, G. A. *Phys. Rev. B* **2001**, *6315*.
(26) Pogantsch, A.; Heimel, G.; Zojer, E. *J. Chem. Phys.* **2002**, *117*, 5921.
(27) Hirata, S.; Lee, T. J.; Head-Gordon, M. *J. Chem. Phys.* **1999**, *111*, 8904.
(28) Stratmann, R. E.; Scuseria, G. E.; Frisch, M. J. *J. Chem. Phys.* **1998**, *109*, 8218.
(29) Neiss, C.; Saalfrank, P.; Parac, M.; Grimme, S. *J. Phys. Chem. A* **2003**, *107*, 140.
(30) Cave, R. J.; Castner, E. W. *J. Phys. Chem. A* **2002**, *106*, 12117.
(31) Halasinski, T. M.; Weisman, J. L.; Ruiterkamp, R.; Lee, T. J.; Salama, F.; Head-Gordon, M. *J. Phys. Chem. A* **2003**, *107*, 3660.
(32) Choi, C. H.; Kertesz, M.; Karpfen, A. *J. Chem. Phys.* **1997**, *107*, 6712.
(33) Perpete, E. A.; Champagne, B. *J. Mol. Struct. (THEOCHEM)* **1999**, *487*, 39.

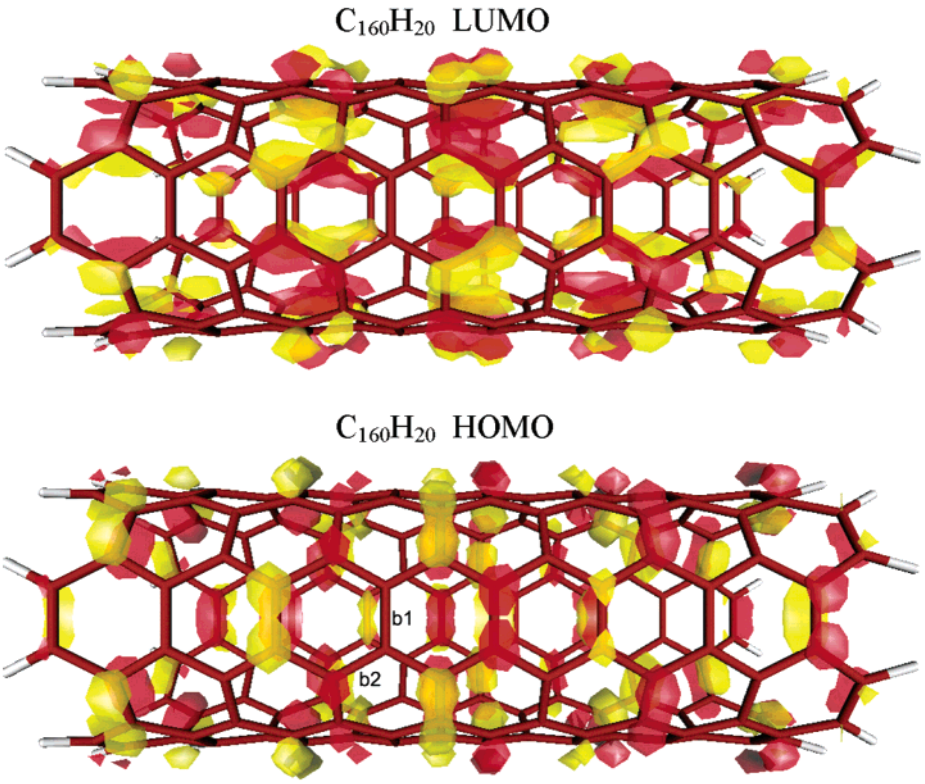


***Figure 2.*** LUMO and HOMO plots of $C_{160}H_{20}$.

Hartree−Fock calculation for the infinite (5,5) tube predicts 1.420 and 1.426 Å for the two types of bond.[34] A very recent PW91 DFT calculation (without exact exchange) predicts a reverse ordering: 1.427 and 1.423 Å for b1 and b2.[35] In both of these cases, there is no variation along the tube length.

Figure 3a shows the optimized lengths of b1 and b2 bonds for neutral $C_{160}H_{20}$, as a function of section number (10 C atoms per section) from one end to the other. Bond alternation is evident in the anti-correlation of b1 and b2. In the center, there is a periodicity of perhaps three or four sections; yet the patterns are not simple, and they vary from molecule to molecule. A three-section periodicity would result from Peierls distortion in the infinite tube.[1] At the tube center, the alternation is ca. 0.017 Å, large as compared to the values quoted above.

In all tubes, the alternation at the tube ends is large and independent of charge state. In $C_{160}H_{20}$, for example, b1 in the two end sections is very short, 1.375 Å, approaching the 1.34 Å value of a localized ethylene double bond. The end hexagons are quite distorted in shape, with almost a full double bond between the two C atoms bonded to H. This bond distortion propagates into the tube center. In Figure 2, the HOMO and LUMO are delocalized in the tube center and have small amplitude on these end ethylenic bonds. These "localized $\pi$ bonds" create occupied and empty "end states" that are significantly below and above the band gap region.

Given the large number of atoms and potentially itinerant electrons in these molecules, the occurrence of low-energy structural isomers is perhaps not surprising. By starting the optimization from different initial structures, we found a second

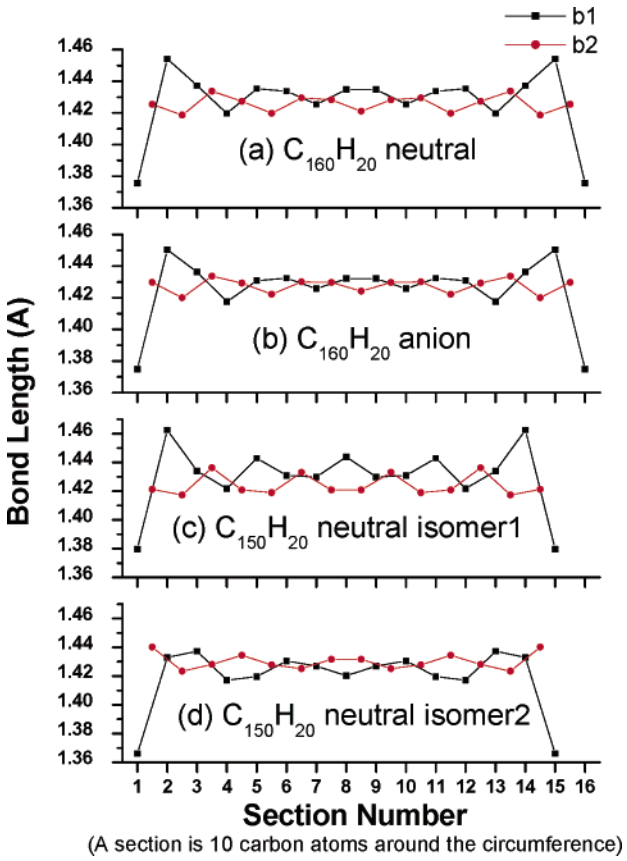


***Figure 3.*** Bond alternation as a function of section number: (a) $C_{160}H_{20}$ neutral, (b) $C_{160}H_{20}$ anion, (c) $C_{150}H_{20}$ isomer1 neutral, (d) $C_{150}H_{20}$ isomer2 neutral.

set of isomeric ground-state structures for the low band gap species $C_{120}H_{20}$, $C_{150}H_{20}$, and $C_{180}H_{20}$. Figure 3c and 3d shows

(34) Tanaka, K.; Ago, H.; Yamabe, T.; Okahara, K.; Okada, M. *Int. J. Quantum Chem.* **1997**, *63*, 637.
(35) Sun, G. Y.; Kurti, J.; Kertesz, M.; Baughman, R. H. *J. Phys. Chem. B* **2003**, *107*, 6924.

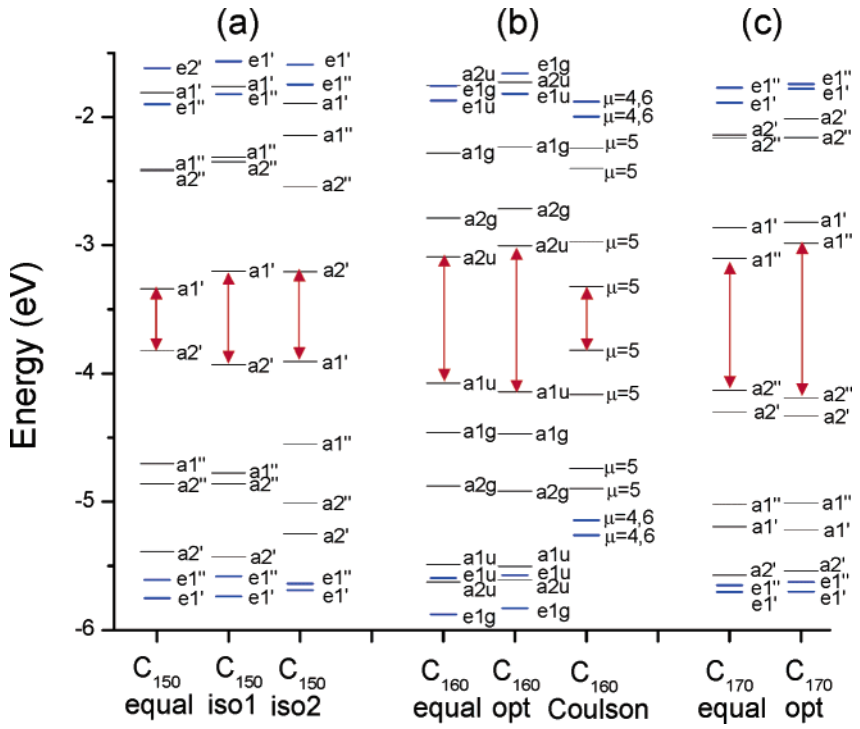


***Figure 4.*** Frontier molecular orbitals for $C_{150}H_{20}$, $C_{160}H_{20}$, and $C_{170}H_{20}$. "opt" refers to optimized geometry, and "equal" refers to equal bond length geometry without bond alternation. In "equal", the common bond length was optimized for lowest energy. "iso" refers to isomer. "Coulson" refers to MO levels from the Coulson model. Coulson MOs are all shifted down 3.57 eV to equalize the Fermi energy. Blue identifies van Hove MOs, and black identifies linear band MOs.

very different bond alternation patterns for the two isomers of $C_{150}H_{20}$; in (c), there is a long (1.46 Å, comparable to the length of 1.467 Å for the $C_2-C_3$ bond in 1,3-butadiene[36]) b1-type near the tube ends, and more pronounced alternation than in (d). These two isomers have essentially the same energy at the present level of calculation. Figure 4a shows that the two isomers in static DFT differ in exchange of the HOMO and LUMO. In $C_{150}H_{20}$, both isomers have band gaps about 50% larger than they would be without bond alternation. For $C_{120}H_{20}$, $C_{150}H_{20}$, and $C_{180}H_{20}$, we have chosen to include the (c) type isomer in the general tables, as the bond alternation pattern is more similar to the other lengths.

Figure 4 compares MO energies near the Fermi energy in the completely optimized alternating structure and an equal bond length structure which is also optimized with constraint of equal bond length for three species. The optimized structures with bond alternation have somewhat larger HOMO−LUMO gaps than the equal bond length structures. In a few places, the ordering of the MOs changes. In $C_{160}H_{20}$, the total energy of the optimized structure is more stable by 2.39 eV; in $C_{170}H_{20}$, it is more stable by 2.45 eV. While the effect is small on a per bond basis, it is quite significant for the entire molecule. In the longest tubes, the alternation is relatively constant in magnitude across the tube center, as is shown for $N = 19$ and $N = 20$ in Figure S1, Supporting Information. In Figure 5a, the magnitude of the bond alternation near the tube center is plotted versus length. While the magnitude does decrease with length, the decay is not monotonic. Vibronic interaction distorting the tube from graphitic structure increases in $C_{120}H_{20}$, $C_{150}H_{20}$, and near $C_{180}H_{20}$ where the static HOMO−LUMO gaps are especially small. This is analogous to Jahn−Teller and Peierls vibronic interaction, although no point symmetry is broken.

In addition to being correlated to the degree of bond alternation, the pattern of band gap maxima and minima is strongly correlated with stability. We define the relative stability for addition of a section of 10 C atoms as $E_{rel}(N) = E(N) - E(N-1) - E_{ave}$. Here, $E(N)$ is the total energy of the H capped molecule with $N$ sections, and $E_{ave} = -10\,370.80$ eV is the average value of $E(N) - E(N-1)$ in the range 3−21. A negative (positive) value of $E_{rel}(N)$ implies that the $N$ section molecule has a greater (lesser) bonding energy per C atom than the $E(N-1)$ molecule. Comparison of Table 1 and Figure 5b shows that higher band gap molecules have stronger bonds, and lower band gap molecules have weaker bonds, when compared to their neighbors in the $N$ sequence. This correlation between band gap and stability makes perfect sense in view of the principle of maximum hardness developed by Parr, Pearson, and Zhou.[37−39] The principle of maximum hardness states that "at equilibrium, chemical systems are as hard as possible". In finite approximation and molecular orbital theory, chemical hardness is proportional to the HOMO−LUMO gap.

The increasing alternation in small gap species, and the occurrence of multiple alternation structures, suggests the possibility that some Peierls-like bond alternation will remain (with a small band gap) in the infinite (5,5) tube. Calculations for unit cells larger than 20 C atoms (necessary for Peierls distortion) with geometrical optimization have not been done, to our knowledge. An STM measurement at low temperature shows a small gap for (8,8) tubes in bundles, but not for single tubes on substrates.[40]

(36) Haugen, W.; Traetteb, M. *Acta Chem. Scand.* **1966**, *20*, 1726.

(37) Parr, R. G.; Chattaraj, P. K. *J. Am. Chem. Soc.* **1991**, *113*, 1854.
(38) Parr, R. G.; Zhou, Z. X. *Acc. Chem. Res.* **1993**, *26*, 256.
(39) Pearson, R. G. *Acc. Chem. Res.* **1993**, *26*, 250.

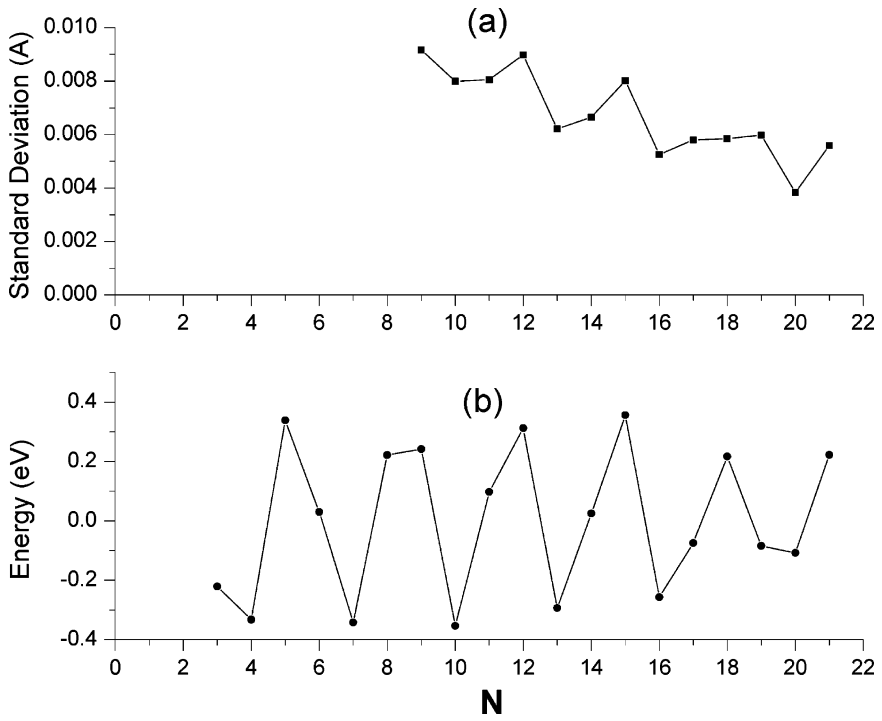


***Figure 5.*** (a) Standard deviation of bond length in tube centers. Here, standard deviation is calculated over all C−C bonds other than three b1 sections and three b2 sections at both ends. (b) Relative stabilization energy as a function of *N* (negative values mean more stable).

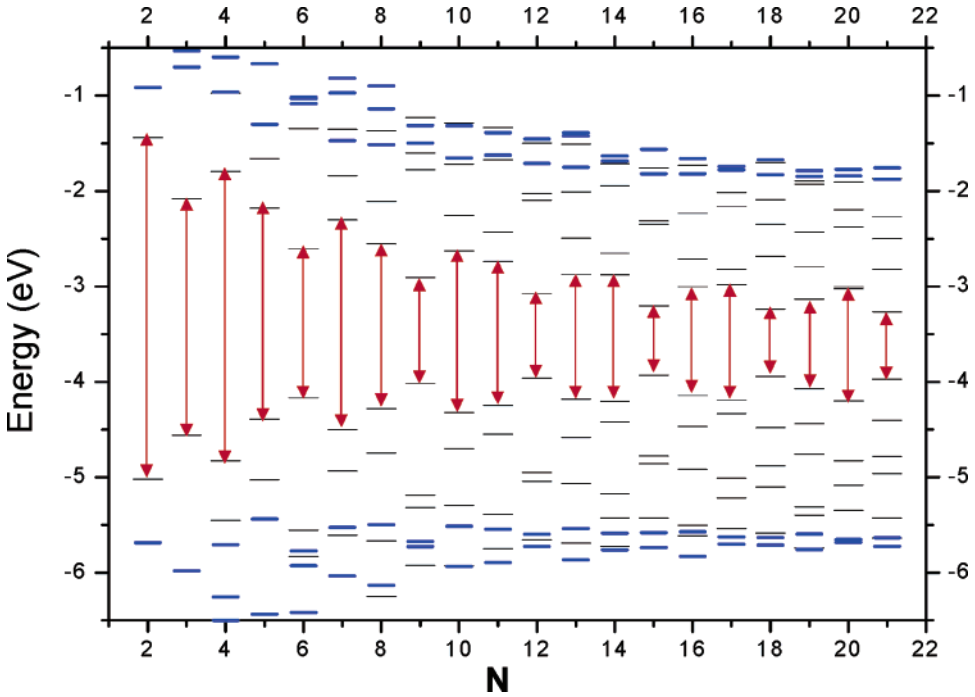


***Figure 6.*** Molecular orbital pattern as a function of *N*. Blue refers to van Hove states, and black refers to linear crossing band states.

After our calculations were complete, a paper on B3LYP optimized structures (assumed $D_5$ geometry) for $C_{120}H_{20}$ and shorter species appeared.[41] Similar alternation patterns were found; the second isomer for $C_{120}H_{20}$ was not reported. These patterns are analyzed as Kekule and Clar modified aromatic networks.

**Molecular Orbitals.** Figure 6 shows MO level patterns as a function of *N*; Figure 4 shows specific MO symmetries for $C_{150}H_{20}$, $C_{160}H_{20}$, and $C_{170}H_{20}$. The high molecular symmetry helps us to identify the infinite tube band parentage of specific MOs. The nondegenerate $\mu = 5$ crossing linear bands yield four different irreducible nondegenerate symmetry species ($a_{1g}$, $a_{1u}$, $a_{2g}$, $a_{2u}$ in $D_{5d}$) MOs. Similarly, the $\mu = 4,6$ degenerate van Hove bands yield four different degenerate symmetries ($e_{1g}$, $e_{1u}$, $e_{2g}$, $e_{2u}$ in $D_{5d}$).

We first discuss the degenerate e-type van Hove MOs. Both the lowest empty and the highest occupied levels drift irregularly to lower energy as *N* values increase and are placed asymmetri-

(40) Ouyang, M.; Huang, J. L.; Cheung, C. L.; Lieber, C. M. *Science* **2001**, *292*, 702.
(41) Matsuo, Y.; Tahara, K.; Nakamura, E. *Org. Lett.* **2003**, *5*, 3181.

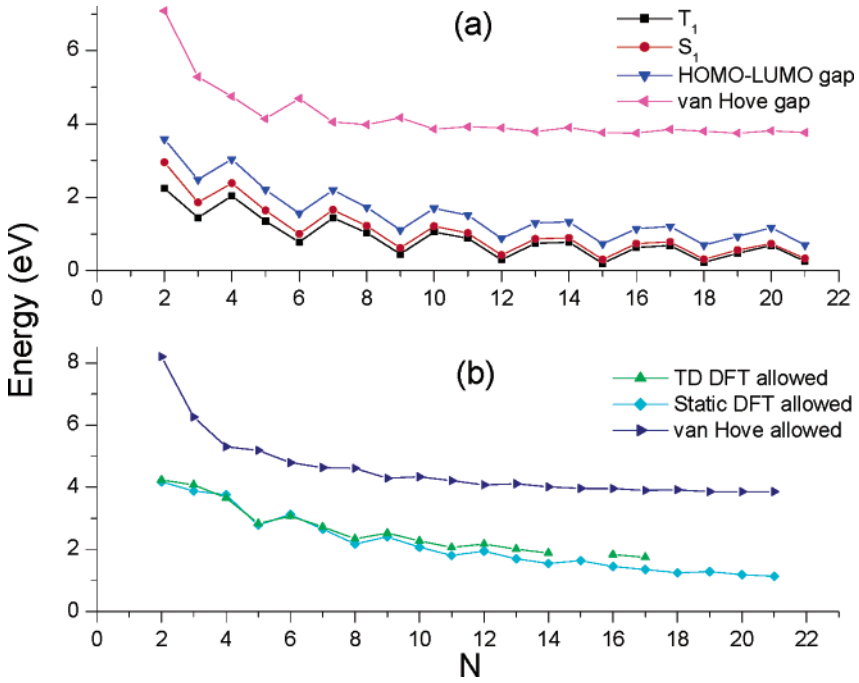


***Figure 7.*** The gaps and excitation energies as a function of *N*.

cally about the HOMO−LUMO gap. The irregularity can be understood as the degree of mismatch between the Coulson momenta $2J\pi/(N+1)a$ and the Fermi momentum $0.673\pi/a$, as discussed in the Introduction. The asymmetry is due to the finite curvature of the tube.[42] The average drift to lower energy by both occupied and unoccupied states is not the behavior expected in a simple quantum size effect involving parabolic bands; the empty levels should move down, and the occupied levels should move up. In our calculation, both occupied and unoccupied states are slowly stabilizing (moving lower) with length, and the gap between them in Figure 7a at first decreases, but then becomes nearly independent of length at 3.8 eV for $N > 15$. In the actual molecules, the structure is changing and stabilizing as unit cells are added; this is not considered in the simple Coulson model. The van Hove energetic gap has almost formed in the calculation. Nevertheless, the high density of states expected at the van Hove edge has not yet formed.

In contrast to the van Hove gap, the gap (due to finite length) between linear crossing band MOs is still very far from closing, as has been noted previously.[10−13] The number of nondegenerate linear band MOs between the van Hove e states increases with *N* as expected. The occupied and unoccupied orbitals occur in symmetric pairs below and above the Fermi energy as predicted in Figure 1. In an important earlier work, Li, Zhang, and Zhang[43] mathematically analyzed the HOMO and LUMO Hückel symmetry patterns as standing waves related to the linear band wave functions of the infinite armchair (5,5) SWNT.

In Figure 4b, we compare the Coulson quantum size effect MOs for $C_{160}H_{20}$ with the DFT MOs. While the pattern is correct, the van Hove separation and the HOMO−LUMO gap are too small. The small van Hove separation suggests that the commonly assumed Hückel resonance integral 2.7 eV used to plot this figure is too small by about 15%. The small gap, however, points out another problem. The DFT calculation finds HOMO−LUMO minima at $N = 3$, 6, 9, 12, 15, 18, and 21. The Coulson factor $2J/(N+1)$ actually predicts minima at $N = 2$, 5, 8, 11, etc. The periodicity is correctly predicted, but the value of *N* for the minima in the gaps has slipped. Physically, this difference probably reflects the fact that carbon sections on both ends are strongly distorted which alters the delocalization of the p electrons near the tube ends. A further generalization of the Coulson model would include a phase shift to account for this effect. Also, the band structure including the curvature effect[3] for the infinite (5,5) tube does not place the Fermi wavevector at exactly $^2/_3$ of the zone boundary; this also affects the detailed pattern of HOMO−LUMO gap oscillations for the finite length tubes.

**Predicted Optical Spectra.** As we previously noted, B3LYP HOMO−LUMO gaps are often good approximations for the lowest excited electronic state. Nevertheless, TD-DFT excitation energies more closely predict optical spectra in aromatic molecules. Figure 7a shows that the TD-DFT lowest triplet and singlet excited states mimic the HOMO−LUMO gap as a function of *N*, running a fraction of an eV lower in energy. Because the spatial components of the open-shell spin−orbitals of the lowest excited singlet and triplet states are essentially identical, the splitting between these two states is due primarily to the difference in exchange energy. Because these open-shell orbitals are increasingly delocalized as *N* increases, the exchange-dominated state splitting should decrease with increasing *N*, as we observe.

The lowest singlet excited TD-DFT states in Figure 7a, as well as many other optical transitions below the van Hove gap, have zero oscillator strength. This can be understood by consideration of the static MO symmetries. In $C_{180}H_{20}$, for example, the forbidden $a_{1g}$ HOMO to $a_{2g}$ LUMO corresponds to the $J = 6$ pair in Figure 1. Actually, all transitions between symmetric pairs of occupied and unoccupied levels of the same *J* are forbidden because the direct vertical band to band ($\Delta k =$

(42) Blase, X.; Benedict, L. X.; Shirley, E. L.; Louie, S. G. *Phys. Rev. Lett.* **1994**, *72*, 1878.
(43) Li, J. Q.; Zhang, Y. F.; Zhang, M. X. *Chem. Phys. Lett.* **2002**, *364*, 328.

***Table 2.*** Lowest Allowed Transitions of (5,5) CNT Fragments from Different Methods[a]

| | static DFT | | TD-DFT | |
|---|---|---|---|---|
| *N* | transition energy (eV) | oscillator strength | transition energy (eV) | oscillator strength |
| 2 | 4.18 | 1.54 | 4.24 | 1.77 |
| 3 | 3.88 | 1.67 | 4.08 | 2.16 |
| 4 | 3.76 | 0.67 | 3.66 | 0.15 |
| 5 | 2.79 | 0.71 | 2.83 | 0.24 |
| 6 | 3.12 | 1.64 | 3.07 | 0.87 |
| 7 | 2.65 | 1.44 | 2.72 | 0.50 |
| 8 | 2.18 | 1.50 | 2.35 | 0.65 |
| 9 | 2.41 | 2.09 | 2.53 | 0.81 |
| 10 | 2.07 | 2.17 | 2.27 | 1.07 |
| 11 | 1.81 | 2.25 | 2.07 | 1.32 |
| 12 | 1.95 | 2.83 | 2.18 | 1.55 |
| 13 | 1.70 | 3.06 | 2.01 | 1.94 |
| 14 | 1.55 | 2.99 | 1.89 | 2.30 |
| 15 | 1.64 | 3.58 | | |
| 16 | 1.45 | 3.94 | 1.84 | 3.13 |
| 17 | 1.36 | 3.80 | 1.75 | 3.65 |
| 18 | 1.25 | 3.89 | | |
| 19 | 1.29 | 4.72 | | |
| 20 | 1.19 | 4.63 | | |
| 21 | 1.14 | 4.59 | | |

[a] All calculations were done at the 6-31g* level.

0) continuous absorption, which would be $a_{1g}$ to $a_{1u}$ in $D_{5d}$,[44] is not allowed in the infinite (5,5) tube.

However, at slightly higher energy, and well below the van Hove gap, we find each molecule has a very strong transition polarized along the tube axis. In static DFT, this transition is a close pair of transitions, from the HOMO to the next MO above the LUMO ($a_{1u}$ to $a_{2g}$ for $C_{160}H_{20}$), and from the next level below the HOMO to the LUMO ($a_{1g}$ to $a_{2u}$). Figure 4 shows the energies and symmetries for three molecules. These transitions are nonvertical $\Delta J = 1$ transitions across $k_F$ in Figure 1. In TD-DFT, the transition appears as one resonance. Figure 7b and Table 2 give transition energies and oscillator strengths as a function of *N*. The TD-DFT results for this lowest allowed intense transition are very close to the static DFT result,[45] running within a few tenths of an eV as a function of *N*. These transitions increase in oscillator strength as *N* increases; for example, the TD-DFT oscillator strength of this 1.75 eV transition in $C_{170}H_{20}$ is 3.65. These *N*-specific, intense transitions should be prime signatures for identification of these tubular molecules in the future. Optical properties have been previously calculated for a couple of short (5,5) sections using the empirical Su−Schrieffer−Heeger model Hamiltonian with graphite-like parameters.[46] PM3 calculations have been reported by Liang et al.[47] These calculations also show this intense transition below the van Hove gap.

Interestingly, the periodicity of three that is observed for the forbidden band gap is almost absent in these allowed transitions. This traces to the $\Delta J = 1$ character of the transitions; $\Delta J = 1$ is the minimum change in momentum along the tube axis allowed for the finite length tube. This scales smoothly to zero as the length of the tube increases. These transitions are allowed

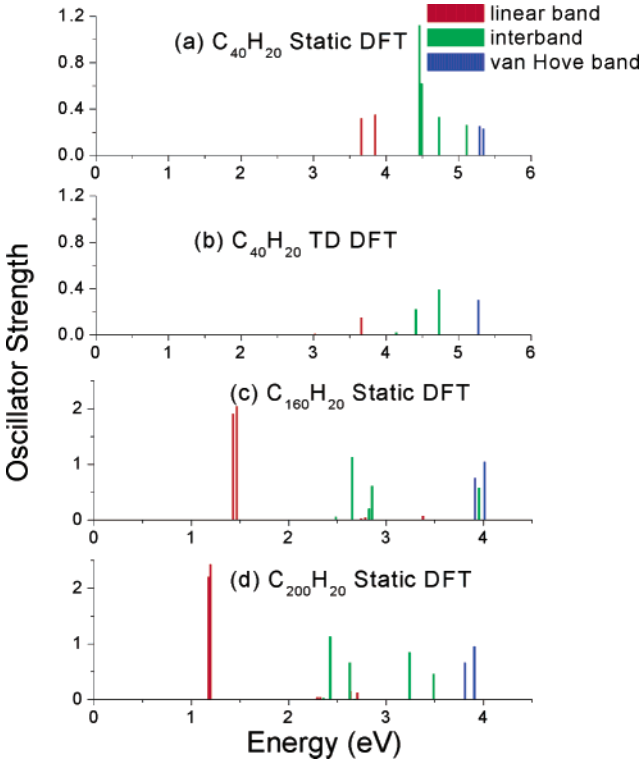


***Figure 8.*** Calculated optical spectra for $C_{40}H_{20}$, $C_{160}H_{20}$, and $C_{200}H_{20}$ from static DFT and TD-DFT. Linear and van Hove band transitions polarized along the tube axis; interband transitions polarized perpendicular to the axis.

due to the finite length of the tubes and increase in oscillator strength as *N* increases. The induced dipole spans the length of the tube. For longer tubes, this transition should move smoothly into the zero frequency pole seen in the real part of the conductivity in metals. In homonuclear diatomic molecules, Mulliken[48] analyzed an analogous class of intense bonding to antibonding electronic transitions as axial end-to-end "charge transfer" in nature. The atmospheric ultraviolet cutoff Shumann−Runge $O_2$ transition is an example. We will refer to this transition in tubular armchair molecules as "charge transfer".

TD-DFT calculations on these large molecules with many different excited states tax our computational abilities. We have not been able to do TD-DFT calculations high enough in energy to reach the van Hove transitions near 4 eV except in the smaller molecules. Figure 8a and 8b shows the complete predicted optical spectra for $C_{40}H_{20}$. For this specific molecule, the TD-DFT calculation slightly increases the intensity of the van Hove edge as compared to the linear band transition; transition energies are not strongly affected. Figure 8c and 8d shows the static DFT predicted optical spectra for $C_{160}H_{20}$ and $C_{200}H_{20}$, respectively. Besides the intense visible "charge transfer" transition, and the van Hove transitions, these figures show that there are also allowed transitions, labeled "interband" in green, from the linear cross bands to the van Hove bands. These vertical ($\Delta k = 0$) transitions, polarized perpendicular to the tube axis, should also occur in the infinite tube but have not yet been experimentally identified.

An approach to metallic behavior is seen in the length dependence of the static axial ground-state polarizability. In standard perturbation theory, ground-state polarizability per

(44) Infinite tube band symmetries taken from Figure 5 of ref 2.
(45) This agreement is similar to the previously mentioned good agreement between the static DFT (with B3LYP) optical transitions and the experimental optical spectra of bulk crystals.
(46) Jiang, J.; Dong, J. M.; Wan, X. G.; Xing, D. Y. *Phys. Lett. A* **1998**, *241*, 274.
(47) Liang, W. Z.; Wang, X. J.; Yokojima, S.; Chen, G. H. *J. Am. Chem. Soc.* **2000**, *122*, 11129.
(48) See: Herzberg, G. *Spectra of Diatomic Molecules*, 2nd ed.; van Nostrand: Princeton, 1950; p 384.

molecule along the tube axis $z$ is related to transition dipoles and optical spectra via[49]

$$\alpha_{zz} = \frac{2}{3h}\sum_{b}\frac{\nu_{ba}|(a|z|b)|^2}{\nu_{ba}^2 - \nu^2} \qquad (1)$$

Here, the sum is over all allowed $z$ polarized transitions and, in our case, is dominated by the low-lying "charge transfer" transitions. Table 1 shows the calculated polarizability per molecule. The periodicity of the band gap is not present in the polarizability because the band gap transitions are forbidden, and the allowed transition varies smoothly with length. The polarizability divided by length is proportional to the static dielectric constant along the axis. Figure S2 in the Supporting Information shows that this ratio increases rapidly with $N$; the larger $N$ molecules begin to behave as near metallic cylindrical objects.

**Charged Nanotubes: Fermi Energy, Capacitance, and Chemical Hardness.** In the most elementary cluster model, the ionization potential of a small metal or semiconductor particle differs from the negative of the bulk Fermi energy ($-E_f$) by a classical charging energy, plus a quantum size effect term.[50,51] The charging energy by itself at high particle dielectric constant gives a correction to the ionization potential $I_p = -E_f + e^2/2R$, and to the electron affinity $E_a = -E_f - e^2/2R$. Here, $R$ is the cluster radius. The ionization potential is larger than the electron affinity, as is the normal situation for molecules. For very small clusters, the electron affinity may even become negative. The quantum size effect term is related to the development of continuous bands from MOs, as we have seen for the HOMO−LUMO gap from the linear crossing bands. If the bands are parabolic, as is the case in the van Hove carbon nanotube transition, and also in 3D semiconductor nanocrystals, then the quantum size effect can be calculated as an effective mass confinement energy. More generally, there is also a contribution to the ionization potential and electron affinity due to structural changes. First, the neutral molecule is distorted from the ideal graphene derived tube structure. This influences the vertical ionization potential and electron affinity. Second, there is the change in the structure induced by the change of the charge state of the molecule. This is the difference between the vertical and the adiabatic ionization potential and electron affinity, which is defined as the reorganization energy of an extra hole and electron in Table 1. For large $N$ in our species, these structural effects are rather small.

The discrete electron approximation for the Fermi energy of any species is $E_f = -(I_p + E_a)/2$, where $I_p$ and $E_a$ are calculated as differences in total energies for the neutral and charged species.[52] In the case of the classical charging model above, we see directly how $E_f$ is recovered by this definition. In carbon nanotubes, we are interested in how $I_p$ and $E_a$ evolve to the work function ($-E_f$) of the infinite length metallic tube. In the context of charging models as discussed above, metallic nanotubes are an interesting case: both the charging energy and the quantum size effect for the linear crossing bands should scale as $1/L$. In the well-studied model of spherical semiconductor nanocrystals, charging scales as $1/R$ while the quantum size effect scales as $1/R^2$. There is also the influence of the structural distortion driven by the termination of the tube to form the finite molecule. As discussed above, the distortion is largest at the ends, decaying into the center of the longer molecules, so one would expect the influence on $E_f$ to decay with length. Finally, the reorganization energies are also expected to scale as $1/L$. The contribution of the reorganization energy to $E_f$ is $-(\lambda_e - \lambda_h)/2$ with the sign conventions of Table 1.

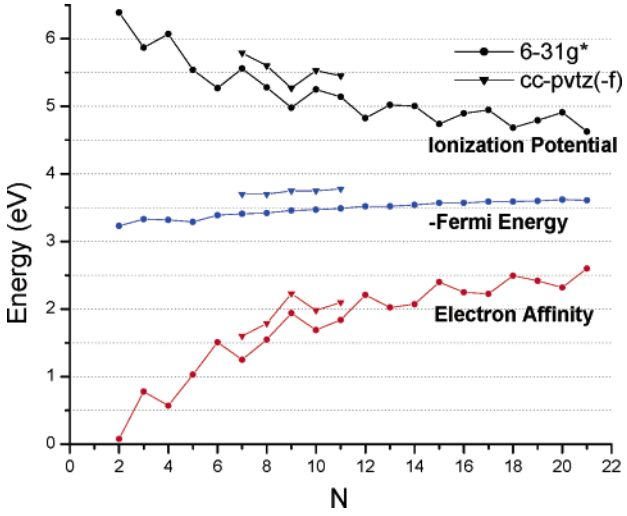


***Figure 9.*** Ionization potential $I_p$, electron affinity $E_a$, and Fermi energy $E_f$ as a function of $N$.

Figure 9 shows $I_p$, $E_a$, and $E_f$ as a function of $N$. Overall, $I_p$ decreases and $E_a$ increases with $L$ as the tubes apparently approach metallic behavior. The values for individual $N$ are anti-correlated and show oscillations that exactly follow the static DFT band gaps. In the context of the simple models, the oscillations are not charging energy variations: the capacitive charging energy of a cylinder should vary smoothly with length.

These oscillations are quantum size effects in $I_p$ and $E_a$, for linear rather than parabolic bands. It is very interesting that these oscillations are anti-correlated and thus cancel out in $E_f$. This occurs because the HOMO and LUMO are symmetric below and above the Fermi energy. In terms of single electron energies with respect to $E_f$, if an electron is removed from the HOMO, the energy change is the same as when an electron is added to the LUMO. In Figure 9, the anti-correlated quantum size effects are smaller than the average difference between $I_p$ and $E_a$, which thus must be mostly due to charging energy.

Because both quantum and charging terms cancel to first order in $-(I_p + E_a)/2$, the Fermi energy is almost constant as a function of $N$. To check predictive accuracy, we have also calculated these energies with the cc-pvtz(-f) basis set in the region $N = 7-11$. Both $I_p$ and $E_a$ increase by about 0.25 eV. This small change supports the validity of working with the 6-31g* basis in general. With this small correction, $E_f$ is about $-3.9$ eV above $N = 15$ and is increasing with length very slowly. This value is suggested to be close to the Fermi energy of an infinite (5,5) tube. Systematic work function measurements of SWNTs have not been reported; there is one UPS report of 4.8 eV for an unspecified tube.[53]

(49) Eyring, H.; Walter, J.; Kimball, G. *Quantum Chemistry*; Wiley and Son: New York, 1944; eq 8-63.
(50) Brus, L. E. *J. Chem. Phys.* **1983**, *79*, 5566.
(51) Makov, G.; Nitzan, A.; Brus, L. E. *J. Chem. Phys.* **1988**, *88*, 5076.
(52) Kohn, W.; Becke, A. D.; Parr, R. G. *J. Phys. Chem.* **1996**, *100*, 12974.
(53) Suzuki, S.; Bower, C.; Watanabe, Y.; Zhou, O. *Appl. Phys. Lett.* **2000**, *76*, 4007.

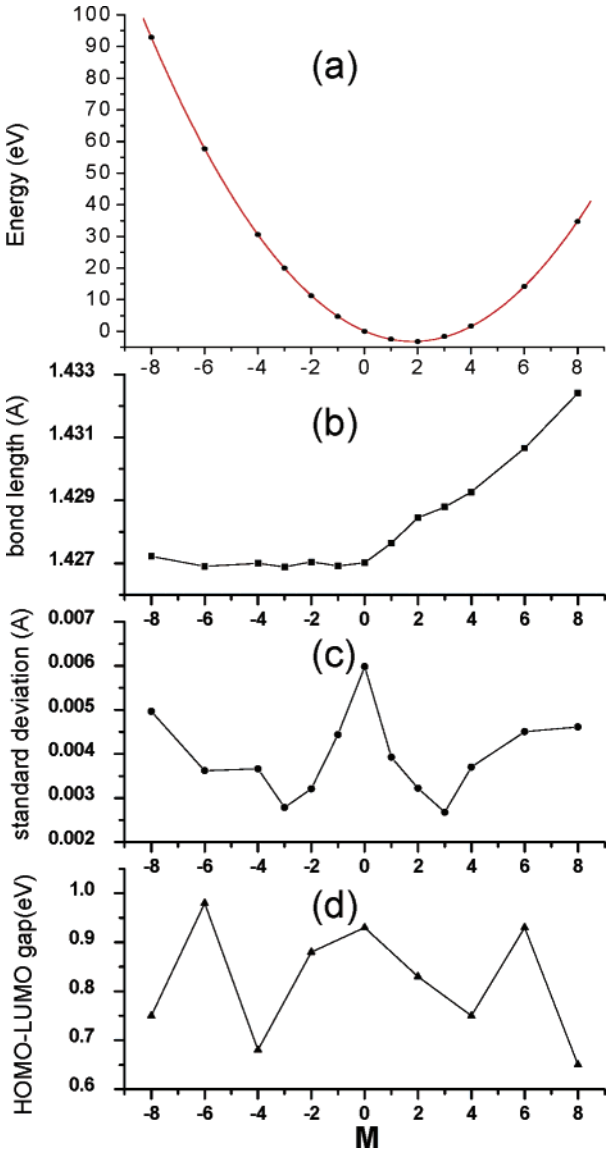


***Figure 10.*** Properties of charged $C_{190}H_{20}$ as a function of $M$ (the number of extra electrons): (a) total energy, (b) the average C−C bond length over all C−C bonds other than three b1 sections and three b2 sections at both ends, (c) the standard deviation due to alternation in the tube center (as in Figure 5a), and (d) the optimized HOMO−LUMO gap.

The Taylor expansion of total electronic energy as a function of the number of extra electrons $M$ (note $M$ is negative for an ionized species) is[54]

$$E(M) = E_o + E_f * M + {}^1/_2\eta M^2 + \ldots\ldots \quad (2)$$

Here, $E_o$ is the energy of the neutral species. The chemical hardness $\eta$ is $I_p - E_a$ (always positive in the cluster model) in the discrete electron approximation. In analyzing $\eta$, there are three generally recognized effects. First, for a closed-shell molecule, there is the difference in the orbital energies for the HOMO and LUMO. Second, there is a charging energy $U$. Finally, there is the influence of structural relaxation.

$$\eta = (\epsilon_{LUMO} - \epsilon_{HOMO}) + U - (\lambda_e + \lambda_h) \quad (3)$$

Note that the (positive) relaxation energies subtract from the chemical hardness. Under some circumstances, relaxation energies can dominate, leading to the possibility of a negative $\eta$, or negative "effective $U$". This occurs for some defects in semiconductors.[55] However, for our molecules, the reorganization energies are minor; the chemical hardness, like the Fermi energy, is dominated by band gap and charging energies. While the finite length quantum size effects and charging energies both cancel to first order in $E_f$, they both add in $\eta$. In Table 1, $\eta$ decreases from near 5 eV for short tubes to 2.03 eV for $C_{210}H_{20}$. In contrast to $E_f$, $\eta$ shows a pronounced periodicity as a function of length, tracking the static HOMO−LUMO periodicity.

If one terminates the Taylor expansion at second order, $E(M)$ is parabolic. A GGA DFT calculation of E(M) was reported in 2002 on a multiply charged $N = 13$ (5,5) section (without geometrical optimization) with $C_{60}$ type end caps.[56] That total energy plot is closely parabolic over a wide range. In Figure 10a, we plot our $E(M)$ for $C_{190}H_{20}$; in each charge state, the structure is reoptimized. These results include the quantum size effects, the structural distortion and relaxation energies, in addition to charging. Over a range of 16 elementary charges, the plot is closely parabolic with a best fit Fermi energy $E_f = -3.63$ eV and hardness $\eta = 1.99$ eV. For the discrete electron approximation involving only the $M = \pm 1$ states, we have $E_f = -3.59$ eV and $\eta = 2.27$ eV from the adiabatic $I_p$ and $E_a$ of $C_{190}H_{20}$. The hardness values are about 15% different. The wide charge range hardness is dominated by the charging energy for the higher charge states; for the singly charged states, both quantum size effect and charging energy contribute. The $M = \pm 1$ low charge points are slightly off the parabolic best fit.

The chemical hardness generally measures the energy required for the tube to store charge. In the cluster charging model, the hardness $I_p - E_a$ equals $e^2/R$ using the equations given above. This is twice the charging energy of a classical metallic sphere in a vacuum. As was also recognized by Luo et al.,[56] the parabolic approximation is very good for larger $N$ values because it physically corresponds to a classical charging model. In the absence of quantum size effect, the total energy of a metallic object of capacitance $C$ is

$$E(M) = E_o + E_f * M + (eM)^2/2C. \quad (4)$$

Comparison with eq 2 suggests that, when charging energy dominates, the chemical hardness predicts an effective capacitance through $\eta = e^2/C$. This simple formula was apparently first proposed by Perdew.[57] The limits and shape aspects of relating capacitance to hardness have been analyzed in detail by Sabin et al.[58] In Figure S3 of the Supporting Information, we plot the capacitance per unit length, $C/L = e^2/(\eta L)$, versus $L$. This plot, using $\eta$ values from Table 1, shows oscillation due to the quantum size effect as it slowly approaches a presumably constant capacitance for large $N$. Actually, the shorter tubes have higher "capacitance" per unit length. For small $N$, the molecules are three-dimensional objects in which the large HOMO−LUMO gap controls $C/L$.[59] For large $N$, the

(54) Equation 3.7 of ref 52.

(55) Anderson, P. W. *Phys. Rev. Lett.* **1975**, *34*, 953.
(56) Luo, J.; Peng, L. M.; Xue, Z. Q.; Wu, J. L. *Phys. Rev. B* **2002**, 66.
(57) Perdew, J. P. *Phys. Rev. B* **1988**, *37*, 6175.
(58) Sabin, J. R.; Trickey, S. B.; Apell, S. P.; Oddershede, J. *Int. J. Quantum Chem.* **2000**, *77*, 358.
(59) In an analogous situation, $\eta$ is called the "quasiparticle band gap" in the semiconductor nanocrystal literature when the HOMO−LUMO gap dominates.

gaps are small, the charge is delocalized, and the cylindrical structure does not vary much with charging; hence, the classical capacitance model works well.

We previously discussed bond alternation as a function of length in the neutral molecules. Figure 10 shows (b) the average bond length, (c) the standard deviation in the tube center due to alternation, and (d) the optimized HOMO−LUMO gap as a function of the number of extra electrons $M$ for $C_{190}H_{20}$. As the tube becomes negatively charged, there is an increase in the average bond length. The bond alternation is relatively large for $M = 0$, and large $|M|$; it shows minima at $M = +3$ and $-3$ charges. This weakly correlates with the HOMO−LUMO gaps. While the bond alternation does vary with $M$, the effect is not large enough to prevent the classical charging model (Figure 10a) from fitting the data well. Note also the electron and hole reorganization energies are very small for large $N$ values in Table 1; the change in bond alternation with a single added charge is small.

**Acknowledgment.** This work has been supported primarily by the Nanoscale Science and Engineering Initiative of the National Science Foundation under NSF Award CHE-0117752 and by the New York State Office of Science, Technology, and Academic Research (NYSTAR). M.S. is supported by the Columbia MRSEC under NSF DMR-02113574. L.E.B. is partially supported by the DOE Basic Energy Sciences under DOE FG02-98ER14861. This work was supported in part by the National Computational Science Alliance under grant MCA95C007N and utilized the IBM P690. A portion of the research described in this paper was performed in the Environmental Molecular Sciences Laboratory, a national scientific user facility sponsored by the Department of Energy's Office of Biological and Environmental Research and located at Pacific Northwest National Laboratory.

**Supporting Information Available:** Bond alternation of $C_{190}H_{20}$ and $C_{200}H_{20}$; the ratio of polarizability divided by the length of tubular molecules as a function of $N$; capacitance per unit length of tubular molecules as a function of length; energies and symmetries of the frontier molecular orbitals of all tubular molecules described in the text. Radiative lifetimes and oscillator strengths of the lowest transitions of the tubular molecules (PDF). This material is available free of charge via the Internet at http://pubs.acs.org.

JA039294P